HHS Public Access

Author manuscript

Nat Metab. Author manuscript; available in PMC 2019 July 07.

Published in final edited form as:

Nat Metab. 2019 January ; 1(1): 158–171. doi:10.1038/s42255-018-0011-x.

Mitochondrial complex III is necessary for endothelial cell proliferation during angiogenesis

Lauren P. Diebold[1], **Hyea Jin Gil**[2], **Peng Gao**[3], **Carlos A. Martinez**[4], **Samuel E. Weinberg**[1], and **Navdeep S. Chandel**[1,*]

[1]Departments of Medicine and Robert H. Lurie Cancer Center, Northwestern University Feinberg School of Medicine, Chicago, IL 60611

[2]Center for Vascular and Developmental Biology, Feinberg Cardiovascular Research Institute, Northwestern University, Chicago, IL 60611

[3]Robert H. Lurie Cancer Center Metabolomics Core, Northwestern University Feinberg School of Medicine, Chicago, IL 60611

[4]Department of Biochemistry and Molecular Genetics, Northwestern University Feinberg School of Medicine, Chicago, IL 60611

Abstract

Endothelial cells (ECs) require glycolysis for proliferation and migration during angiogenesis; however, the necessity for the mitochondrial respiratory chain during angiogenesis is not known. Here we report that inhibition of respiratory chain complex III impairs proliferation, but not migration of ECs *in vitro* by decreasing the NAD+/NADH ratio. To determine whether mitochondrial respiration is necessary for angiogenesis *in vivo*, we conditionally ablate a subunit of the respiratory chain complex III (QPC) in ECs. Loss of QPC decreases respiration, resulting in diminished EC proliferation, and impairment in retinal and tumor angiogenesis. Loss of QPC does not decrease genes associated with anabolism or nucleotides levels in ECs, but diminishes amino acid levels. Our findings indicate that mitochondrial respiration is necessary for angiogenesis, and that the primary role of mitochondria in ECs is to serve as biosynthetic organelles for cell proliferation.

*Corresponding author: nav@northwestern.edu.

AUTHOR CONTRIBUIONS

L.D. carried out the majority of experiments and data analysis. P.G. performed the HPLC-MS/MS metabolite analysis. C.A.M. analyzed the RNA sequencing data. H.J.G. and S.E.W. provided intellectual and technical expertise. L.D. and N.S.C. provided intellectual input and wrote the paper.

COMPETING FINANCIAL INTERESTS

The authors declare no competing financial interests

DATA AVAILABILITY

All data from this manuscript are available from the corresponding author upon request. RNA sequence data that support the findings of this study have been deposited in GEO with the accession code GSE121770. https://www.ncbi.nlm.nih.gov/geo/query/acc.cgi?acc=GSE121770.

INTRODUCTION

While largely quiescent in healthy adult tissues, endothelial cells (ECs) are dynamic, undergoing rapid migration and proliferation during angiogenesis; thus, increasing their biosynthetic and bioenergetic demand. Recent findings indicate that metabolism is a critical regulator of EC function during angiogenesis. ECs are classically described as being highly glycolytic, and numerous studies have described the necessity of glycolysis in ECs during vessel sprouting [1]. Despite having abundant access to oxygen in the bloodstream, ECs generate up to 85% of their ATP from glycolysis [2]. When vessel sprouting is stimulated by pro-angiogenic signals such as vascular endothelial growth factor A (VEGFA), glycolysis is enhanced due to upregulation of glycolytic enzymes, nearly doubling flux through glycolysis [2–4]. This increased glycolytic flux is critical, as decreased expression of the glycolytic activator phosphofructokinase-2/fructose-2,6-bisphosphatase (PFKFB3), severely impairs both migration and proliferation of ECs *in vitro* and *in vivo* [2]. Furthermore, inhibition of PFKFB3 in ECs decreased pathological neovascularization in ocular and inflammatory models, as well as cancer cell metastasis [5,6]. Moreover, decreased levels of other glycolytic enzymes including hexokinase 2 (HK2), pyruvate kinase M2 (PKM2), and glucose transporter 1 (GLUT1) cause impaired angiogenesis [7–9]. Collectively these data indicate that glycolytic flux in ECs is necessary for angiogenesis.

Since ECs undergo high levels of aerobic glycolysis, and thus oxidize only small amounts of glycolysis-derived pyruvate within the mitochondria, mitochondrial function was previously surmised to play a marginal role in EC metabolism [2]. In addition to importing glucose, ECs take up fatty acids from their environment and break them down into acetyl-CoA in the mitochondria in a process known as fatty acid oxidation (FAO). Fatty acid-derived acetyl-CoA is then utilized to fuel the tricarboxylic acid (TCA) cycle [10]. FAO has been shown to be critical in ECs, as knock down of fatty acid binding protein 4 (FABP4) or carnitine palmitoyltransferase 1A (CPT1A) leads to diminished angiogenesis [11–13]. Glutamine is also readily imported into ECs where it is metabolized into alpha-ketoglutarate (αKG), which is used to replenish the mitochondrial TCA cycle (i.e. anaplerosis). Limiting EC glutamine utilization results in diminished angiogenesis both *in vitro* and *in vivo* [14,15]. While FAO and glutamine utilization fuel metabolism during vessel sprouting, loss of either of these two pathways result in a relatively modest decrease in angiogenesis compared to inhibition of PFKFB3. It is likely that restricting one particular carbon source to fuel the TCA cycle will not markedly impair mitochondrial metabolism.

In the present study, we directly tested the necessity for mitochondrial metabolism during angiogenesis by inhibiting the mitochondrial respiratory chain complex III. Respiration is initiated by the donation of electrons to complexes I and II by the TCA cycle-generated reducing equivalents NADH and $FADH_2$, respectively. Mitochondrial complexes I and II pass electrons to complex III, and finally to oxygen via complex IV. This electron flow drives the pumping of hydrogen ions into the intermembrane space to generate membrane potential required for ATP production by ATP synthase (complex V). Respiration is linked to three distinct mitochondrial functions: (1) oxidative phosphorylation for ATP generation; (2) oxidative TCA cycle flux to produce metabolites for macromolecule biosynthesis; and (3) release of reactive oxygen species (ROS) and metabolites to determine cell fate and/or

function. Thus, loss of mitochondrial complex III could have multiple effects on cells, including death due to a bioenergetic collapse, decreased proliferation due to diminished oxidative TCA cycle function for macromolecule synthesis, and loss of cell fate and/or function due to changes in angiogenic gene expression. Thus, we utilized mitochondrial complex III inhibitors *in vitro*, and an EC-specific mitochondrial complex III-deficient mouse model to test which mechanisms linked to mitochondrial respiration in ECs are required for angiogenesis.

Here, we conclude that *in vitro*, mitochondrial complex III is necessary for EC proliferation but not migration, and is critical for maintenance of the NAD+/NADH ratio. Conditional loss of complex III (QPC) in ECs *in vivo* diminishes retinal, lung, and tumor angiogenesis by decreasing EC proliferation. While anabolic gene signaling is maintained, loss of QPC in ECs *in vivo* results in reduced amino acid levels. Overall, we conclude that mitochondrial complex III is required for angiogenesis, and in ECs the principal role of mitochondria is to act as signaling organelles to support proliferation.

RESULTS

Mitochondrial complex III is required for endothelial cell proliferation *in vitro*

To study the effects of mitochondrial respiratory chain inhibition on EC behavior, we cultured human umbilical vein endothelial cells (HUVECs) with the mitochondrial complex III inhibitor antimycin A to induce loss of mitochondrial respiration (Fig. 1a). Since respiratory capacity was abolished, we confirmed that HUVECs were performing maximal glycolysis basally (Fig. 1b). Importantly, even after 96 hours of treatment with antimycin A in culture, no significant decrease in cell viability was observed, indicating that respiratory chain inhibition does not cause HUVEC death or apoptosis (Fig. 1c and Supplementary Figs. 1a-1b). Furthermore, antimycin A treatment does not lead to mitochondrial demise *in vitro*, as we observed no loss of mitochondrial membrane potential, mitochondrial content, or mitochondrial DNA (Supplementary Fig. 1c-1i). Two important processes activated in ECs in response to angiogenic signaling are sprouting (i.e. invasion and migration) and proliferation [16]. We therefore utilized HUVECs in culture to explore how mitochondrial inhibition affects these key angiogenic functions. First, we used an *in vitro* sprouting assay where HUVEC spheroids sprout and migrate through a 3D collagen matrix. After 24 hours, spheroids treated with antimycin A showed no changes in sprout length or number (Figs. 1d-1f). Additionally, respiration-deficient HUVECs migrated similar to controls in a 2D scratch wound migration assay (Fig. 1g). Interestingly, HUVECs treated with antimycin A displayed a striking defect in proliferation, as they completely failed to grow over a period of 96 hours (Fig. 1h). Similar results were obtained when HUVECs were treated with the mitochondrial complex I inhibitor, piericidin (Supplementary Fig. 2). Together, these data clearly show that the mitochondrial respiratory chain is necessary for HUVEC proliferation *in vitro*, while it is dispensable for migration and sprouting.

Mitochondrial complex III maintains NAD+/NADH ratio, necessary for endothelial cell proliferation

The mitochondrial TCA cycle is critical for cellular proliferation, as it produces metabolic intermediates that are used as building blocks for biosynthetic macromolecules [17]. Metabolic profiling revealed that respiration-deficient HUVECs displayed decreased levels of TCA cycle intermediates (Fig. 2a). Broadly, amino acid levels in HUVECs treated with antimycin A were not impaired, with the exception of aspartate, which was significantly decreased (Fig. 2b). Nucleotide metabolite abundance remained relatively unchanged in respiration-deficient HUVECs (Supplementary Fig. 3a and 3b). To test specificity of antimycin A, we expressed the *Ciona intestinalis* alternative oxidase (AOX) in HUVECs, which is refractory to antimycin treatment [18,19]. AOX has the capability to accept electrons from ubiquinol and transfer them to oxygen, bypassing complex III and IV functions, and restoring electron transport chain activity in the presence of complex III inhibition [18,19]. We found that HUVECs expressing AOX maintain oxygen consumption and NAD+/NADH in the presence of antimycin A, indicating that AOX is functioning properly (Figs. 2c and 2d). Importantly, AOX was able to rescue proliferative capacity after antimycin A treatment, as it restores both TCA cycle metabolites and aspartate levels (Figs. 2e-2g). Together, these data highlight the specificity of antimycin A, and demonstrate that its effects on HUVECs are due to its inhibition of complex III.

Cells use complex I of the ETC to oxidize NADH to NAD+; thus, after complex III inhibition, there is a decreased capacity to regenerate NAD+, causing decreased TCA cycle flux. Previously it has been demonstrated that restoration of NAD+/NADH is sufficient to rescue proliferation in respiration-deficient cancer cells [20,21]. To test this hypothesis in HUVECs, we expressed an NADH oxidase from *Lactobacillus brevis* (LbNOX) which generates NAD+ from NADH independent of ETC function [21]. We found that expressing LbNOX in the cytosol did not restore OCR, but was able to rescue NAD+/NADH, and proliferation in antimycin A treated HUVECs (Figs. 2h-2j). Additionally, respiration-deficient HUVECs expressing LbNOX accumulate large amounts of succinate, due to complex III inhibition (Fig. 2k). Finally, expressing LbNOX in antimycin A treated HUVECs was able to increase aspartate levels relative to EV (Fig. 2l). These data indicates that an essential function of the ETC in HUVECs is to maintain NAD+/NADH to support cellular proliferation.

Numerous studies have reported that cells lacking a functional respiratory chain are able to proliferate *in vitro* upon supplementation with supra-physiological levels of pyruvate in the culture media [20,22,23]. Similarly, we observed that addition of methyl pyruvate (MP), while not rescuing OCR, was able to restore proliferative capacity in antimycin A treated HUVECs (Supplementary Figs. 3c and 3d). Additionally, antimycin A treated HUVECs with MP accumulated succinate due to complex III inhibition and displayed restored aspartate levels (Supplementary Figs. 3e and 3f). As aspartate levels are decreased in antimycin A treated HUVECs and are rescued upon expression of AOX, LbNOX or addition of MP, we hypothesized that supplementation with aspartate would allow proliferation after ETC inhibition. Previous studies have reported that in respiration deficient cancer cells, aspartate is sufficient to support proliferation in the absence of pyruvate [20,22]. Surprisingly,

aspartate was not able to rescue proliferation in antimycin A treated HUVECs (Supplementary Fig. 3g). Additionally, neither cell permeable methyl aspartate nor asparagine (which is converted to aspartate by the enzyme asparaginase) were able to restore proliferation (Supplementary Fig. 3h and 3i). Together, these data reveal that in HUVECs, mitochondrial complex III fulfills biosynthetic requirements by supporting NAD+ regeneration. It is likely that NAD+ dependent aspartate synthesis is necessary but not sufficient for cell proliferation.

Inhibiting mitochondrial complex III respiration in HUVECs does not broadly disrupt histone modifications

In addition to fulfilling a biosynthetic demand, mitochondrial metabolites have recently been shown to be necessary to maintain histone acetylation [24,25]. Accumulation of the TCA cycle intermediates succinate and fumarate, as well as the metabolite L-2-hydroxyglutarate (2HG), leads to competitive inhibition of alpha-ketoglutarate (αKG)-dependent dioxygenases, including JmJC domain-containing histone lysine demethylases (KDMs) and the ten-eleven translocation (TET) family of 5-methlycytosine (5mC) hydroxylases [26,27]. Recently, we reported that build-up of these three metabolites in mitochondrial complex III KO hematopoietic stem cells, resulted in hyper-methylation of DNA and histones [24]. In the present study, we unexpectedly observed a decrease in 2HG, as well as the expected increase in 2HG:αKG, Succinate:αKG, and Fumarate:αKG (Supplementary Figs. 3j-3m). Others have reported that fatty acid oxidation is necessary to maintain H3K9 acetylation in lymphatic endothelial cells [28]. However, we found that histone modifications in HUVECs treated with antimycin A were largely unchanged (Supplementary Fig. 4a). Specifically, we did not observe changes in H3K9 acetylation or methylation, and saw minimal alterations in other major histone marks linked to gene expression (Supplementary Figs. 4b-4f). Together, these data indicate that mitochondrial complex III in HUVECs *in vitro* is not required for maintenance of chromatin modifications.

Mitochondrial complex III respiration in ECs is required for post-natal retinal angiogenesis

The microenvironment and nutrient availability of ECs differs greatly between cell culture and a living organism, prompting us to ask what the requirements are for EC mitochondrial complex III function *in vivo*. To explore the effect of mitochondrial respiratory chain inhibition *in vivo*, we crossed mice with a floxed *Uqcrq* gene, which encodes for ubiquinol binding protein, (a critical subunit of the mitochondrial respiratory chain complex III) ($QPC^{fl/fl}$), with $Cdh5Cre^{ERT2}$ mice, to allow for tamoxifen-inducible, endothelial-specific loss of mitochondrial respiration (QPC-KO) [29].

To understand the role of EC mitochondrial complex III respiration in vessel sprouting *in vivo*, we studied angiogenesis in the post-natal mouse retina. Mouse pups were administered 5 doses of tamoxifen on post-natal days 0–4 (P0-P4) to induce Cre recombination and loss of respiration in ECs. To ensure recombination, QPC-WT and -KO mice were crossed to mice harboring a lox-stop-lox TdTomato allele (Supplementary Fig. 5). Retinal whole mounts from P7 pups stained with isolectin-B4 (IB4) revealed a dramatic impairment in retinal angiogenesis in QPC-KO mice (Fig. 3a). By P7, vessels should nearly reach the outer edge of the retina, however radial expansion was massively impaired in QPC-KO mice, as

vessels only reached about half the distance to the outer retinal edge (Figs. 3a and 3b). Additionally, a striking decrease in vascular density can be observed in QPC-KO retinas, which show substantially fewer branchpoints/mm^2 (Figs. 3a and 3c). Further staining revealed that QPC-KO retinas had significantly fewer phospho-histone 3 (pH3) positive ECs, indicating a proliferative impairment congruent with what was observed *in vitro* (Figs. 1h, 3d, and 3e). Moreover, filopodia of QPC-KO ECs on the outer retinal edge were unremarkable in both appearance and number as compared to QPC-WT, suggesting no defect in migration, again consistent with our *in vitro* data (Figs. 1d-1g, 3f and 3g). Additionally, we did not observe an increase in retinal EC apoptosis (cleaved caspase 3) or vessel regression (empty collagen IV sleeves) in QPC-KO mice compared to WT, indicating that decreased retinal vascularity was not due to EC death or regression (Supplementary Figs. 5b-5e). We conclude that complex III inhibition in vivo, decreases EC proliferation, but does not alter migration, apoptosis, or regression of vessels during post-natal retinal angiogenesis.

Mitochondrial complex III function in ECs is necessary for post-natal developmental angiogenesis

Next, we aimed to uncover whether mitochondrial respiration in ECs is necessary for post-natal pup survival. To answer this question, QPC-WT and -KO pups were given 5 doses of tamoxifen (P0-P4) to induce Cre recombination and loss of QPC in ECs. We observed a striking decrease in survival of QPC-KO pups, the majority of which died between P15 and P30 (Fig. 4a). To further explore vascular defects in this model, lungs were harvested from P15 QPC-WT and -KO pups. We chose to investigate the lung as it contains a large population of ECs, which are actively undergoing angiogenesis at this age, a critical process in post-natal lung alveolarization [30]. QPC-KO lung ECs have diminished expression of QPC mRNA, and displayed decreased OCR and NAD+/NADH ratio, indicating a loss of respiratory chain function (Supplementary Figs. 6a – 6c). QPC-KO pups showed no obvious signs of distress or decline in body weight at P15 (Fig. 4b). However, flow cytometric analysis of homogenized P15 lungs revealed a significant reduction in both the percentage and total number of ECs, consistent with a decrease in lung angiogenesis (Figs. 4c, 4d, and Supplementary Fig. 6d). Recall that *in vitro*, as well as in the retina, mitochondrial respiratory chain complex III inhibition caused reduced proliferation (Fig. 1h, 3d, and 3e). Likewise, pH3 staining of P15 lungs revealed a decrease in EC proliferation (Figs. 4e and 4f). Taken together, these data show that loss of mitochondrial complex III leads to a significant defect in lung angiogenesis.

Loss of mitochondrial complex III function in ECs increases anabolic-associated gene expression

Although we did not observe profound changes in histone methylation or acetylation in respiration-deficient HUVECs (Supplementary Fig. 4), we wondered whether loss of mitochondrial respiration in ECs would lead to gene deregulation *in vivo*. Thus, we harvested lung ECs from QPC-WT and -KO P15 pups treated with tamoxifen (P0-P4), and performed RNA-sequencing analysis. We observed modest alterations in gene expression, with 237 upregulated and 142 downregulated genes in QPC-KO ECs as compared to QPC-WT (FDR ≤ 0.01) (Fig. 5a). Surprisingly, gene set enrichment analysis revealed a significant

upregulation in pathways associated with anabolism and cellular proliferation, including MYC, MTORC, E2F, and G2M target signaling (Fig. 5b). We also observed an increase in the unfolded protein response (UPR), a cellular stress response that has been shown to be activated upon loss of mitochondrial respiratory function [31] (Fig. 5b). Ribosomal biosynthesis genes are critical targets of cellular pro-growth signaling [32]. Indeed, we found that a substantial percentage (21%) of the significantly upregulated genes in QPC-KO ECs were ribosomal genes, further corroborating intact proliferative signaling (Fig. 5c). QPC-KO ECs show several significantly increased metabolic genes including those regulating glycolysis, one-carbon metabolism, and the urea and TCA cycles (Fig. 5d). Additionally, QPC-KO ECs display a trend toward increased oxidative phosphorylation genes, likely a compensatory mechanism due to massive loss of mitochondrial function (Fig. 5e). These data indicate that although QPC-KO ECs have decreased proliferation, they maintain anabolic gene expression.

Interestingly, RNA-seq revealed a handful of key angiogenic signaling genes that were significantly altered in QPC-KO ECs (Fig. 5f). Specifically, hairy/enhancer-of-split related with YRPW motif protein 1 (Hey1), delta-like 4 (Dll4), and TEK receptor tyrosine kinase (Tek, aka Tie2) were significantly downregulated, while neuropilin-2 (Nrp2), and angiopoitin-2 (Angpt2) were significantly upregulated in QPC-KO ECs (Fig. 5f). Validation of our RNAseq data at the protein level revealed increased metabolic protein expression, but no change in angiogenic protein expression (Supplementary Figs. 7). Our data suggest that ECs lacking mitochondrial complex III have impaired proliferation and angiogenesis yet retain anabolic gene expression.

Mitochondrial complex III in ECs is necessary to maintain amino acid levels *in vivo*

As anabolic signaling remained intact in QPC-KO ECs, we hypothesized that a metabolic deficiency was preventing proliferation. Metabolite analysis revealed decreased levels of numerous metabolites in the QPC-KO ECs as compared to QPC-WT (Fig. 6a). We did not observe an accumulation of 2HG, however, the TCA cycle metabolites fumarate and malate were significantly lower in QPC-KO ECs, as were several glycolytic intermediates (Figs. 6b and Supplementary Fig. 8). Intriguingly, the majority of the metabolites decreased in QPC-KO ECs were amino acids (Fig. 6a). In contrast to HUVECs *in vitro*, where amino acid levels were maintained with the exception of aspartate, QPC-KO lung ECs displayed significantly diminished levels of nearly all amino acids (Figs. 6a and 6c). Purine and pyrimidine nucleotide levels, however, remained largely unchanged upon loss of EC respiration (Figs. 6d and 6e). Together, these results suggest that mitochondrial complex III in ECs is required to maintain amino acid levels, but not nucleotides, which could lead to the impaired proliferation observed in QPC-KO ECs.

Mitochondrial complex III function in ECs is required for tumor angiogenesis

To further investigate the role of EC respiration and determine its requirement in adult mice, we asked whether mitochondrial respiration in ECs is required for tumor angiogenesis. 8-week old adult QPC-WT and QPC-KO mice were fed tamoxifen chow for 2 weeks to induce Cre recombination and loss of QPC mRNA expression and respiration in ECs (Figs. 7a and 7b). Next, we subcutaneously injected syngeneic B16-F10 melanoma cells into the mice and

measured tumor volume over the course of 21 days. QPC-KO mice showed a decrease in tumor growth as compared to QPC-WT, and by days 19 and 21 harbored significantly smaller tumors (Fig. 7c). On day 21, when tumors were harvested, QPC-KO mice also displayed a reduction in tumor weight (Fig. 7d). Histological analysis revealed that QPC-KO tumors had fewer vessels per area, indicating decreased tumor angiogenesis (Figs. 7e and 7f). Consistent with data from the retina and lung, tumor ECs proliferated less, suggesting that impaired tumor angiogenesis is likely due to reduced EC proliferation (Figs. 7g and 7h). These data suggest that mitochondrial complex III function is required in adult ECs in order to sustain tumor angiogenesis and tumor growth.

DISCUSSION

Endothelial cells exhibit high levels of flux through glycolysis, only oxidizing a small fraction of glucose-derived carbons in the mitochondria [2,15]. Accordingly, limiting glycolysis profoundly impairs angiogenesis [2,5–9]. By contrast, the function of mitochondrial metabolism in ECs is not fully understood. Here we report that pharmacological inhibition of mitochondrial respiratory transport chain complex III in ECs impairs cell proliferation by decreasing NAD+/NADH *in vitro*. Conditional loss of respiratory chain complex III in ECs *in vivo* diminished post-natal retinal, lung, and tumor angiogenesis. Our results conclusively demonstrate that mitochondrial respiratory chain complex III is necessary for angiogenesis by controlling EC cell proliferation. These results fill a critical gap in knowledge about the role of the mitochondrial respiratory chain in ECs, a classically glycolytic cell type in which mitochondrial metabolism has largely been underappreciated. Our results indicate that angiogenesis requires coordination of both glycolysis and mitochondrial respiratory chain linked metabolism. It is likely that this coordination in ECs occurs through MYC, since loss of MYC specifically in ECs impairs glycolysis, mitochondrial metabolism and proliferation [33].

Mitochondria serve three main functions within a cell: (1) they generate ATP via oxidative phosphorylation for cell survival; (2) the TCA cycle generates metabolic intermediates that produce critical macromolecules required for cell growth, including amino acids, nucleotides and lipids; and (3) mitochondria act as signaling organelles, generating reactive oxygen species (ROS) to activate transcriptional networks and produce metabolic intermediates that control epigenetics. The major phenotype we observed due to mitochondrial complex III function impairment is diminished cell proliferation *in vitro* and *in vivo*. This defect is likely not due to lack of mitochondrial ATP production as it has been suggested that ECs generate up to 85% of their ATP though glycolysis alone [2]. Additionally, complex III loss in ECs did not impair ATP demanding activities such as sprouting and migration *in vitro* or filopodia formation *in vivo,* further highlighting that glycolysis can alone provide sufficient ATP for these processes. Our data are consistent with previous studies showing that glycolysis drives filopodia formation and migration in ECs [2].

The proliferative impairment observed in complex III deficient ECs *in vitro* and *in vivo* is likely due to the inability to generate the necessary metabolites for macromolecule synthesis. Previous studies in cancer cells *in vitro* have demonstrated that loss of complex III decreases NAD+ levels, resulting in diminished aspartate, which is necessary for cancer cell

proliferation [20,22]. In cancer cells treated with complex III inhibitors, restoration of NAD+ levels, either by supplementation with pyruvate or by genetic expression of NAD+ regenerating enzymes, restores aspartate levels and cell proliferation *in vitro* [20,21]. Congruently, *in vitro*, we observed decreased NAD+/NADH and diminished aspartate levels in respiration-deficient HUVECs. As previous studies have shown, supplementation with pyruvate restored proliferation after ETC inhibition as well as aspartate levels. Additionally, we found that genetically increasing the ratio of NAD+/NADH was sufficient to rescue proliferation and aspartate in antimycin A treated HUVECs, which is again consistent with *in vitro* cancer cell data [21]. Intriguingly, unlike cancer cells, aspartate was not able to restore proliferation in respiration deficient ECs *in vitro*, perhaps due to distinct metabolic programming between cancer and primary cells. It is important to note that proliferation of not all cancer cell lines is sensitive to aspartate limitation [34]. Additionally, cancer cells differ in their ability to uptake aspartate, and have varied asparaginase activity [35]. We suggest that perhaps aspartate is not sufficient to support proliferation in HUVECs. However, NAD+/NADH ratio, which is linked to other metabolic functions beyond restoring aspartate levels, is sufficient to support HUVEC proliferation.

Additionally, we found that ECs *in vivo* lacking complex III function not only had diminished NAD+/NADH and aspartate levels, but also decreased abundance of the majority of amino acids. It is not clear why amino acid levels were markedly diminished from complex III deficient ECs. Gene set enrichment analysis revealed an unexpected increase in anabolic gene expression profiles in QPC-KO ECs, with an increase in genes linked to MYC and mTORC1, including upregulated ribosomal gene expression. This increase in anabolic programs would impose a high demand for amino acids. Thus, in the absence of a functional respiratory chain, the TCA cycle metabolites are not able to maintain amino acid levels to keep up with the increased anabolic demand, resulting in diminished growth. Previously, we observed that gene set enrichment analysis from mitochondrial complex III deficient hematopoietic stem cells (HSCs) similarly displayed upregulation of MYC and mTORC1 linked genes [24]. Going forward it will be important to decipher how loss of mitochondrial complex III function causes an increase in MYC and mTORC1 related genes *in vivo*.

Although our present data on ECs indicate that respiratory chain linked metabolism is necessary for cell proliferation, it is not a universal feature of proliferating cells. For example, fetal mouse HSCs do not require mitochondrial complex III for cell proliferation, but to generate sufficient progenitor populations *in vivo* [24]. Moreover, adult mouse complex III deficient HSCs lose quiescence and undergo stem cell exhaustion; thus, complex III is required for HSCs to function properly [24]. Mitochondrial complex III deficient HSCs display deregulated expression of approximately 1000 genes, concomitant with histone H3K4, H3K9, and H3K79 hyper-methylation [24]. These changes were accompanied by increased levels of succinate, fumarate, and 2HG, metabolites known to inhibit α-KG-dependent dioxygenases including KDMs and TETs [24,26,27]. We hypothesized that we would see these same trends in ECs, however we did not observe accumulation of neither succinate, fumarate, nor 2HG *in vivo.*

Although, the mitochondrial complex III deficient ECs did not display widespread deregulation of gene expression, there were a few angiogenic associated genes altered,

including those involved in the Notch signaling pathway (Dll4 and the two downstream targets Hey1 and Hes1) *in vivo*. Previous studies have shown that Notch signaling is critical for angiogenesis both *in vitro* and *in vivo* [2,36]. Specifically, decreased Notch signaling in HUVECs accelerated sprouting, while constitutive Notch activation had the opposite effect [2]. In a mouse model, pharmacological inhibition of Notch signaling with the inhibitor DAPT, or genetic ablation through conditional knockout of the Notch ligand Dll4 in ECs, increased branching and tip cell formation in the retina[36]. In our *in vivo* model, loss of complex III in ECs lead to decreased Notch signaling, however we observed decreased branching, contrary to what has been observed upon loss of Notch signaling in ECs. As loss of Notch signaling has been found to have the opposite phenotype as diminished respiration in ECs, we conclude that decreased Notch signaling is likely not the dominant factor that leads to impaired angiogenesis in out model. Additionally, mitochondrial complex III deficient ECs display decreased mRNA expression of Tie2, along with overexpression of the Tie2 negative regulator Angpt2, suggesting decreased signaling through Tie2 in QPC-KO ECs. However, we observed no concomitant change in Tie2 or Angpt2 protein levels suggesting no alterations in Tie2 signaling. Overall, we conclude that mitochondrial complex III's dominant function in ECs is to sustain amino acid availability for cell proliferation *in vivo*.

Our observation that complex III linked metabolism in ECs is necessary for cell proliferation is similar to observations in cancer cells. Previously, both others and we have demonstrated that pharmacological inhibition or genetic ablation of the respiratory chain within cancer cells diminishes tumorigenesis in part by decreasing cell proliferation [39–48]. This has led to the idea of targeting the respiratory chain for cancer therapy [49]. We observed that inhibition of the respiratory chain, by diminishing complex III in ECs, impaired tumorigenesis. Consequently, administration of respiratory chain inhibitors could work as an anti-cancer therapy through decreasing proliferation of both cancer and endothelial cells. Interestingly, increasing mitochondrial function diminishes prostate tumor vascularization highlighting that mitochondrial homeostasis is crucial for maintaining tumor angiogenesis [50].

METHODS

Cell Culture and drug treatment

Human umbilical vein endothelial cells (HUVECs) (Lonza) were cultured in Endothelial Basal Medium (MCDB 131) without pyruvate (USBiological), and used at a low passage number (1–6) for *in vitro* assays. Media was supplemented with EGM-2 SingleQuot growth factors (Lonza), 1% GlutaMax (Gibco), and 400μM Uridine (supplemented MCDB 131 media). B16-F10 melanoma cells were cultured in RPMI (Corning), with 10% FBS (Corning), 1% sodium pyruvate (Gibco), 1% Non-essential amino acids (Gibco), 1% GlutaMAX (Gibco), 1% antibiotic/antimycotic (Corning), and 0.05mM β-mercaptoethanol (Sigma). Cells were maintained at 37˚C with 5% CO_2. HUVECs were treated with: 25nM Antimycin A (Sigma), 250nM Piericidin (Sigma), 1mM methyl pyruvate (MP) (Sigma), and/or indicated doses of L-Aspartic Acid (aspartate) (Sigma), L-aspartic acid dimethyl ester hydrochloride (methyl aspartate) (Sigma), or L-asparagine (asparagine) (Sigma).

Oxygen consumption and extracellular acidification rate measurements

Oxygen consumption rate (OCR) and extracellular acidification rate (ECAR) were measured using an XF96 extracellular flux analyzer (Seahorse Bioscience).

***In vitro*:** 30,000 HUVECs per well were plated onto XF96 cell culture plates in supplemented MCDB 131 media and allowed to attach for 4 hours. Cells were then treated with mitochondrial respiratory chain inhibitor for 2 hours. Basal respiration was measured by subtracting the OCR values after treatment with 2 μM antimycin A (Sigma) and 2 μM rotenone (Sigma). Coupled respiration was determined by treatment with 2.5 μM oligomycin A (Sigma), and subtracting oligomycin A values from basal respiration. To measure ECAR, cells were treated in supplemented MCDB 131 media without sodium bicarbonate. Basal ECAR was measured by subtracting the ECAR rate after treatment with 20mM 2-deoxyglucose (2-DG) (Sigma). Maximum ECAR rate was measured by subtracting the rate after after 2-DG treatment from the rate after treatment with 2.5uM Oligomycin A.

***In vivo*:** 100,000 lung ECs were plated onto XF96 cell culture plates in supplemented MCDB 131 media and attached using Cell-Tak following the manufacturer's protocol (Corning). Basal respiration was measured by subtracting the OCR values after treatment with 2 μM antimycin A (Sigma) and 2 μM rotenone (Sigma). Coupled respiration was determined by treatment with 2.5 μM oligomycin A (Sigma), and subtracting oligomycin A values from basal respiration.

HUVEC proliferation and viability assays

For proliferation curves, HUVECs were plated in supplemented MCDB 131 media and allowed to attach overnight. The next day (time 0), media was replaced with supplemented MCDB 131 media with or without drug treatments. Cells were then counted at each timepoint (24, 48, 72, or 96 hours) via flow cytometry using AccuCount Fluorescent Particles (Spherotech). For viability, HUVECs were plated and treated as described above. Viability was assessed at 96 hours post-treatment via flow cytometry by adding 100ng/mL of 4',6-Diamidino-2-phenylindole dihydrochloride (DAPI) and assessing the percentage of DAPI negative cells. To measure apoptosis and viability, HUVECs were plated and treated as described above. After 48 or 96 hours, cells were collected and stained with AnnexinV and Propidium Iodide according to the manufacturers protocol (eBioscience AnnexinV apoptosis detection kit).

Measurement of HUVEC mitochondrial membrane potential and content

HUVECs were plated and treated as described above and collected after 48 or 96 hours. To measure membrane potential, cells were stained with 50nM TMRE (Tetramethylrhodamine ethyl ester perchlorate, Molecular Probes) for 20 minutes at 37˚C. Median fluorescence intensity (MFI) (PE) was measured by flow cytometry and corrected by subtracting the MFI of each sample after addition of 25uM CCCP (carbonyl cyanide m-chlorophenyl hydrazine). To measure mitochondrial content, cells were stained with 25nM MitoTracker Green (Molecular Probes) for 20 minutes at 37˚C. MFI (FITC) was measured by flow cytometry.

qRT-PCR and western blot analysis

To measure QPC expression, RNA was isolated using the E.Z.N.A Total RNA Kit I by following the manufacturer's protocol (Omega). CYBRFast 1-Step RT-qPCR Lo-ROX Kit (Tonbo) was used to measure QPC expression with the following primers: QPC-F: 5'-GAGACTGAGGATATCGATTG-3', and QPC-R: 5'- GGATGCGCTCGCGAGTGCGG-3'. To measure mitochondrial DNA content, genomic DNA was purified using the QIAamp DNA Mini Kit (Qiagen), and qRT-PCR was performed using iQ SYBR Green Supermix (Bio-Rad) using the following primers: ND2-F: 5'-GCCCTAGAAATAAACATGCTA-3'; ND2-R: 5'-GGGCTATTCCTAGTTTTATT-3'; COX2-F: 5'-CTGAACCTACGAGTACACCG-3'; COX2-R: 5'-TTAATTCTAGGACGATGGGC-3'; CYTB-F: 5'-CATTTATTATCGCGGCCCTA-3'; CYTB-R: 5'-TGGGTTGTTTGATCCTGTTTC-3'; SDHA-F: 5'-TCCACTACATGACGGAGCAG-3'; SDHA-R: 5'-CCATCTTCAGTTCTGCTAAACG-3'; b-actin-F: 5'-TCCACCTTCCAGCAGATGTG-3'; b-Actin-R: 5'-GCATTTGCGGTGGACGAT-3'. For western blot analysis, cells were lysed in 1× Cell Lysis Buffer (Cell Signaling) containing PMSF (phenylmethane sulfonyl fluoride). Relative protein abundance was measured using the Wes system (ProteinSimple) using the manufacturer's protocol and the following antibodies: SHMT2 (Cell Signaling, 12762), PHGDH (Abcam, Ab211365), GAPDH (Sigma, G9545), Tie2/TEK (Millipore, 05–584), and Angpt2 (Invitrogen, PA5–23612).

HUVEC sprouting assay

HUVECs were first resuspended in 20% methylcellulose (Sigma, 4000cP viscosity) at a concentration of 1000 cells per 25uL. This suspension was then dropped onto non-adherent plates (25uL drops), flipped upside-down, and HUVECs were allowed to form spheroids overnight in hanging drops. Spheroids were collected in PBS + 10% FBS and spun down at 300×g for 5 minutes and then 500×g for 3 minutes at room temperature with no brake. Spheroids were then resuspended in 40% FBS in methylcellulose, combined with collagen type I (EMD Millipore), $NaHCO_3$, and NaOH, plated, and allowed to polymerize at 37˚C. Wells were then topped with an equal volume of supplemented MCDB 131 media with or without drug treatments. Media contained 2ug/mL mitomycin C (Sigma) to inhibit proliferation. Spheroids were allowed to sprout for 24 hours before fixation with 4% paraformaldehyde.

HUVEC scratch-wound cell migration assay

Scratch-wound cell migration assays were performed using the IncuCyte ZOOM 96-well scratch wounds cell migration system (Essen BioScience). HUVECs were plated onto 96-well Image Lock tissue culture plates (Essen BioScience, 4379) at a density of 30,000 cells per well in supplemented MCDB 131 media and allowed to attach overnight. Cells were then treated with 5ug/mL mitomycin C for 2 hours to inhibit proliferation. Monolayers were then wounded using the 96-well WoundMaker (Essen BioScience) following the manufacturer's protocol. Media was then replaced with supplemented MCDB 131 with or without drug treatments and images of wounds were taken every 4 hours until closure.

Lentiviral constructs

Empty vector (EV) and AOX pWPI GFP [51], or EV and LbNOX pLV-EF1 RFP [21] (VectorBuilder, VB160708–1059xrd) lentiviral constructs were transfected into COS1 cells using jetPRIME transfection reagent (Polyplus), along with pMD2.G and psPAX2 packaging vectors to produce EV-GFP, AOX-GFP, EV-RFP, and LbNOX-RFP lentiviruses. HUVECs were transduced with each lentivirus, and either GFP+ or RFP+ cells were sorted using fluorescence-activated cell sorting (FACS) after 48 hours. Cells were allowed to recover overnight and then plated for each assay.

Mice and tamoxifen administration

C57BL/6 mice harboring a loxp flanked exon 1 of the *Uqcrq* gene (encodes QPC) were generated by Ozgene. Mice were genotyped using the following primers: 1. 5'-CTTCCGCTCCTCCCGGAAGT-3', 2. 5'-TTCCCAAACTCGCGGCCCATG-3' and 3. 5'-CAATTCCAGCCAACAGTCCC-3' which allow identification of the QPC wild-type, loxp-flanked, and excised alleles. QPC-floxed mice were crossed with Cdh5Cre^{ERT2} mice, which have a tamoxifen-inducible Cre allele under the endothelial-specific Cadherin 5 (Cdh5, aka VE-cadherin) promoter [29]. The Cre allele was detected by using the following primers: 1. 5'-AATCTCCCACCGTCAGTACG-3', and 2. 5'-CGTTTTCTGAGCATACCTGGA-3'. Lox-stop-lox TdTomato mice were purchased from Jackson (stock no. 007914). Tamoxifen stock was prepared by dissolving tamoxifen (Sigma) in corn oil by shaking at 37˚C for 2 hours. Tamoxifen was administered to mouse pups orally by dropping 2.5μL of 40mg/mL tamoxifen stock into the mouth using a p10 pipet. Pups were given 5 doses of tamoxifen from P0-P4 at a dose of 100μg/pup/day. For tumor angiogenesis assays, adult mice were fed tamoxifen chow (Envigo) for 2 weeks prior to tumor injection and remained fed with tamoxifen chow for the entirety of the experiment. All animal procedures were approved by the Institutional Animal Care and Use Committee (IACUC) at Northwestern University.

Postnatal retinal angiogenesis assay

Mouse pups were dosed with tamoxifen as described above. Eyeballs were harvested, fixed and retinas were dissected on P7 as previously described [52]. Retinas were blocked/permeabilized in PBS + 5% bovine serum albumin (BSA) (OmniPur) + 0.5% TritonX-100 (Sigma) for 4 hours at room temperature (RT) while rocking. Retinas were then stained with fluorescently labeled primary antibodies overnight at 4˚C, cut into cloverleaves, and whole-mounted onto slides using Prolong Diamond Antifade Mounting Media (Molecular Probes).

Isolation of endothelial cells from mouse lungs

Whole lungs were harvested from QPC-WT and -KO mice dosed with tamoxifen. Lungs were perfused with phosphate buffered saline (PBS) and then with dispase (corning). Lungs were then cut into small pieces using scissors and digested while shaking at 37˚C in 5 mg/mL Collagenase type I (Gibco) and 1 mg/mL DNase I (Roche). Lung tissue was homogenized by passing it though a 28G needle several times, and filtering through a 70um filter. Red cell lysis was performed by resuspending homogenized lung pellets in 1mL of RBC lysis buffer for 2 minutes. For RNAseq, homogenized lungs were stained with biotinylated CD45 and depleted of CD45+ cells using EasySep Mouse Streptavidin

RapidSpheres Isolation Kit (Stemcell) by using the manufacturer's protocol. CD31+ cells were then sorted by FACS. For Metabolomics, Homogenized lungs were stained with both biotinylated CD45 and biotinylated CD326/EpCAM and depleted of CD45+ and EpCAM+ cells using EasySep Mouse Streptavidin RapidSpheres Isolation Kit (Stemcell) by using the manufacturer's protocol. Cells were then stained with CD31-FITC, and CD31+ cells were enriched using the Mouse FITC Selection Kit (Stemcell).

Histological analysis

Tumors were fixed in 4% paraformaldehyde for 24 hours, and submitted for histological analysis. Briefly, organs were paraffin embedded and sectioned onto slides. Following standard deparaffinization, antigen retrieval was performed using pH6 sodium Citrate buffer at 110 degrees C for 20 minutes in a biocare decloaking chamber. Slides were blocked and incubated with primary antibodies overnight at 4˚C. Blocking and secondary antibody steps were performed using an automated Intellipath staining system made by BioCare. Lungs were dissected and perfused though the trachea with a 1:1 solution of optimal cutting temperature (OCT) medium (Fisher), embedded in OCT, and frozen in 2-methylbutane on dry ice. Frozen tissue was cryo-sectioned (7μm) and placed on slides, and fixed with acetone. Briefly, sections were blocked and then incubated with primary conjugated antibodies for 1 hour at room temperature.

Antibodies, flow cytometry, and cell sorting

Lung homogenates were stained with the following antibodies: anti-mouse CD45 biotin (ebioscience, 13–0451-82, clone 30-F11, 1:100), anti-mouse CD326/EpCAM biotin (Invitrogen, 2020–10-01, clone G8.8., 1:100), anti-mouse CD31-FITC (BioLegend, 102406, clone 390, 1:100). For flow cytometry, live cells were gated by staining with GhostDye viability stain (Tonbo Biosciences, 1:200). Retinas were stained with the following antibodies/stains: GS Isolectin-B4 (IB4) (Invitrogen, I21411, Alexa-Fluor 488, 1:100), anti-phospho-histone 3 (Ser10) (Alexa Fluor 647, EMD Millipore, 06–570, polyclonal, 1:400), Collagen IV (Goat, EMD Millipore, AB769, polyclonal, 1:25), Cleaved Caspase-3 (Rabbit, Cell Signaling, 9661, polyclonal, 1:100), Alexa Fluor 647 AffiniPure Bovine Anti-Goat (Jackson Immuno., 805–605-180, 1:500) and DyLight 405 AffiniPure Donkey Anti-Rabbit (Jackson Immuno., 711–475-152, 1:500). Tumors sections were stained with the following antibodies: anti-CD31 (Goat, Santa Cruz, sc-1506, M-20, 1:250), anti-phospho-histone 3 (Ser10) (Rabbit, abcam, ab5176, polyclonal, 1:1000), anti-Goat Cy3 (Jackson Immuno., 1:1000), and anti-Rabbit Alexa-Fluor 488 (Jackson Immuno, 1:1000). Lungs sections were stained with the following antibodies: anti-CD31 (PE-CF594, BD Horizon, 563616, MEC 13.3, 1:100), and anti-phospho-histone 3 (Ser10) (Alexa Fluor 647, EMD Millipore, 06–570, polyclonal, 1:100). Tumors and lung section nuclei were stained with 100ng/mL of 4',6-Diamidino-2-phenylindole dihydrochloride (DAPI). Flow cytometry, samples were run on LSR Fortessa flow cytometers (BD) and data was analyzed using FlowJo software. Cell sorting was performed using the FACS Aria II (BD).

Microscopy and image analysis

Images of HUVEC spheroids were taken using a Nikon AZ100 Multi-purpose Zoom Microscope and Nikon imaging software. Images were analyzed using ImageJ software.

Images of scratch-wound assays were taken every 4 hours using the automated IncuCyte live-cell analysis system (Essen BioScience). Percent wound closure was analyzed and calculated using IncuCyte scratch wound software (Essen BioScience). Retinal, lung, and tumor images were taken using the Nikon A1 Confocal Laser Microscope System and analyzed using ImageJ software. Branchpoint analysis was performed using AngioTool software.

Metabolite analysis

In vitro: HUVECs were plated in supplemented MCDB 131 media and allowed to attach overnight. Media was then replaced with supplemented MCDB 131 media with or without drug and treated for 24 hours. Cells were collected and pellets were flash frozen in liquid nitrogen in cryovials.

In vivo: Endothelial cells were isolated from P15 mouse lungs as described above and pellets were flash frozen in liquid nitrogen. Frozen pellets were stored at −80˚C until extraction.

Metabolite extraction and sample analysis: Samples were thawed and resuspended in 500uL of ice cold 80% methanol (HPLC grade) and subjected to 3 freeze-thaw cycles alternating between liquid nitrogen and a 37˚C water bath. Next, samples were centrifuged at 18,000×g for 10 minutes at 4˚C. The resulting supernatants were transferred to fresh tubes and dried. Samples were resuspended in 10μl per 200,000 cells. Samples were analyzed by High-Performance Liquid Chromatography and High-Resolution Mass Spectrometry and Tandem Mass Spectrometry (HPLC-MS/MS). Specifically, the system consisted of a Thermo Q-Exactive in line with an electrospray source and an Ultimate3000 (Thermo) series HPLC consisting of a binary pump, degasser, and auto-sampler outfitted with an Xbridge Amide column (Waters; dimensions of 4.6 mm × 100 mm and a 3.5 μm particle size). The mobile phase A contained 95% (vol/vol) water, 5% (vol/vol) acetonitrile, 20 mM ammonium hydroxide, 20 mM ammonium acetate, pH = 9.0; B was 100% Acetonitrile. The gradient was as following: 0–1 min, 15% A; 18.5 min, 76% A; 18.5–20.4 min, 24% A; 20.4–20.5 min, 15% A; 20.5–28 min, 15% A with a flow rate of 400 μL/min. The capillary of the ESI source was set to 275 °C, with sheath gas at 45 arbitrary units, auxiliary gas at 5 arbitrary units and the spray voltage at 4.0 kV. In positive/negative polarity switching mode, an m/z scan range from 70 to 850 was chosen and MS1 data was collected at a resolution of 70,000. The automatic gain control (AGC) target was set at 1 × 106 and the maximum injection time was 200 ms. The top 5 precursor ions were subsequently fragmented, in a data-dependent manner, using the higher energy collisional dissociation (HCD) cell set to 30% normalized collision energy in MS2 at a resolution power of 17,500. The sample volumes of 10 μl were injected which contained 200,000 cells. Data acquisition and analysis were carried out by Xcalibur 4.0 software and Tracefinder 2.1 software, respectively (both from Thermo Fisher Scientific). NAD+/NADH ratio was measured using the NAD/NADH-glo Assay (Promega) by following the manufacturer’s protocol.

RNA sequencing analysis

Mouse pups were dosed with tamoxifen and endothelial cells were isolated from P15 mouse lungs as described above. Cells were lysed with RLT buffer + 0.1% β-mercaptoethanol from the RNeasy Plus Micro Kit (Qiagen) and stored at −80˚C until RNA was extracted. RNA isolation were performed using the RNAeasy Plus Micro Kit (Qiagen) following the manufacturer's instructions with an additional on-column DNase treatment using RNase-free DNase Set (Qiagen). RNA quality and quantity were measured using Agilent 4200 Tapestation using high Sensitivity RNA ScreenTape System (Agilent Technologies). NEBNext Ultra™ RNA (New England Biolabs, Inc) was used for full-length cDNA synthesis and library preparation. Libraries were pooled, denatured and diluted, resulting in a 2.0 pM DNA solution. PhiX control was spiked at 1%. Libraries were sequenced on an Illumina NextSeq 500 instrument (Illumina Inc) using NextSeq 500 High Output reagent kit (Illumina Inc) (1×75 cycles) with a target read depth of approximate (8–16) million aligned reads per sample. FASTQ reads were trimmed using Trimmomatic to remove end nucleotides with a PHRED score less than 30 and requiring a minimum length of 20 bp. Reads were then aligned to the mm10 genome using tophat version 2.1.04 using the following options --no-novel-juncs --read-mismatches 2 --read-edit-dist 2 --max-multihits 20 –library-type fr- unstranded. The generated bam files were then used to count the reads only at the exons of genes using htseq-count5 with the following parameters -q -m intersection-nonempty -s no -t exon. Differential expression analysis was done using the R package edgeR6. Bigwig tracks of RNA-Seq expression were generated by using the GenomicAlignments package in R in order to calculate the coverage of reads in counts per million (CPM) normalized to the total number of uniquely mapped reads for each sample in the library. GSEA analysis was done using using the Broad Institute GSEA software7. In brief, the gene list output from edgeR was ranked by calculating a rank score of each gene as –log 10 (PValue)*sign(logFC). A pre-ranked GSEA analysis was done using 3000 permutations and the Hallmark pathway database.

Tumor angiogenesis assay

8 week old mice were dosed with tamoxifen as described above. The right flank was shaved and 100,000 B16-F10 melanoma cells (ATCC) were injected subcutaneously. Tumor size was measured using calipers every 2–3 days for 21 days. According to the approved protocol, tumors were not permitted to exceed 2cm in diameter (approximately $4cm^3$). Tumor volume was calculated by first determining the geometric mean between the length and width, then using the equation: $(4/3)*(\pi)*(\text{geometric mean}/2)^3$. On day 21, tumors were harvested, weighed, tumor size was measured, and volume was calculated using the equation: $(4/3)*(\pi)*(\text{length}/2)*(\text{width}/2)*(\text{depth}/2)$.

Mass spectrometry to identify histone modifications

Nuclei were isolated using gentle detergent treatment (0.3% NP-40 in NIB-250 buffer) of cells and centrifugation at 0.6*g*. Detergent was removed by 2× washing of obtained pellets with NIB-250, no NP-40 buffer. Histones from isolated nuclei were acid-extracted and derivatized with propionic anhydride both prior to and following trypsin digestion as previously described [53]. Propionylated histone peptides were resuspended in 50 μl water

with 0.1% TFA and 3 μl was injected in 3 technical replicates on a nanoLC/triple quadrupole MS that consisted of a Dionex UltiMate 3000 coupled to a Thermo Fisher Scientific TSQ Quantiva triple quadrupole mass spectrometer. Buffer A was 100% LC–MS-grade water with 0.1% formic acid and buffer B was 100% ACN. The propionylated peptides were loaded onto an in-house packed C18 trapping column (4 cm × 150 μm; Magic AQ C18, 3 μm, 200 Å-Michrom) for 10 min at a flow rate of 2.5 μl min^{-1} in 0.1% TFA loading buffer. The peptides were separated by a gradient from 1 to 35% buffer B from 5 to 45 min. The analytical column was 10 cm × 75 μm PicoChip (1PCH7515–105H253-NV New Objective) and consisted of the same C18 material as the trapping column. The triple quadrupole settings were as follows: collision gas pressure of 1.5 mtorr; Q1 peak width of 0.7 (full-width at half-maximum); cycle time of 3 s; skimmer offset of 10 V; electrospray voltage of 2.5 kV. SRM mass spectrometer transitions were developed as described previously [54,55]. Data were analysed using Skyline software (v3.5; MacCoss Lab, University of Washington) with Savitzky–Golay smoothing of peaks [56]. Automatic peak assignment and retention times were checked manually.

Supplementary Material

Refer to Web version on PubMed Central for supplementary material.

ACKNOWLEDGEMENTS

This work was supported by the NIH (R35CA197532, 5P01AG049665 and 5P01HL071643–13) to N.S.C., and NIH (T32 GM08061) to L.P.D. We thank Ralf Adams for $Cdh5Cre^{ERT2}$ mice. Imaging work was performed at the Northwestern University Center for Advanced Microscopy generously supported by NCI CCSG P30 CA060553 awarded to the Robert H Lurie Comprehensive Cancer Center. Histology services for tumor tissue was provided by the Northwestern University Research Histology and Phenotyping Laboratory which is supported by NCI P30-CA060553 awarded to the Robert H Lurie Comprehensive Cancer Center. Analysis of histone modifications was performed by the Northwestern Proteomics Core Facility, generously supported by NCI CCSG P30 CA060553 awarded to the Robert H Lurie Comprehensive Cancer Center and the National Resource for Translational and Developmental Proteomics supported by P41 GM108569. Flow cytometric analysis was supported by the Northwestern University Flow Cytometry Core Facility supported by Cancer Center Support Grant (NCI CA060553). Flow Cytometry Cell Sorting was performed on a BD FACSAria SORP system, purchased through the support of NIH 1S10OD011996–01. Metabolomics services were performed by the Metabolomics Core Facility at Robert H. Lurie Comprehensive Cancer Center of Northwestern University. We would like to thank Hiam Abdala-Valencia and Kiwon Nam for RNA sequencing. Finally, we would like to thank Guillermo Oliver at Northwestern University for his helpful intellectual input.

REFERENCES

1. Teuwen L-A, Geldhof V & Carmeliet P How glucose, glutamine and fatty acid metabolism shape blood and lymph vessel development. *Dev. Biol.* (2017). doi:10.1016/j.ydbio.2017.12.001
2. De Bock K et al. Role of PFKFB3-driven glycolysis in vessel sprouting. Cell 154, 651–663 (2013). [PubMed: 23911327]
3. Parra-Bonilla G, Alvarez DF, Al-Mehdi A-B, Alexeyev M & Stevens T Critical role for lactate dehydrogenase A in aerobic glycolysis that sustains pulmonary microvascular endothelial cell proliferation. *Am. J.* Physiol. Lung Cell. Mol. Physiol. 299, L513–522 (2010). [PubMed: 20675437]
4. Yeh W-L, Lin C-J & Fu W-M Enhancement of glucose transporter expression of brain endothelial cells by vascular endothelial growth factor derived from glioma exposed to hypoxia. *Mol. Pharmacol.* 73, 170–177 (2008). [PubMed: 17942749]
5. Cantelmo AR et al. Inhibition of the Glycolytic Activator PFKFB3 in Endothelium Induces Tumor Vessel Normalization, Impairs Metastasis, and Improves Chemotherapy. Cancer Cell 30, 968–985 (2016). [PubMed: 27866851]

6. Schoors S et al. Partial and transient reduction of glycolysis by PFKFB3 blockade reduces pathological angiogenesis. Cell Metab. 19, 37–48 (2014). [PubMed: 24332967]
7. Boeckel J-N et al. JMJD8 Regulates Angiogenic Sprouting and Cellular Metabolism by Interacting With Pyruvate Kinase M2 in Endothelial Cells. *Arterioscler. Thromb. Vasc.* Biol. 36, 1425–1433 (2016). [PubMed: 27199445]
8. Tang M et al. Brain microvasculature defects and Glut1 deficiency syndrome averted by early repletion of the glucose transporter-1 protein. Nat. Commun 8, 14152 (2017). [PubMed: 28106060]
9. Yu P et al. FGF-dependent metabolic control of vascular development. Nature 545, 224–228 (2017). [PubMed: 28467822]
10. Houten SM & Wanders RJA A general introduction to the biochemistry of mitochondrial fatty acid β-oxidation. *J. Inherit. Metab. Dis.* 33, 469–477 (2010). [PubMed: 20195903]
11. Elmasri H et al. Fatty acid binding protein 4 is a target of VEGF and a regulator of cell proliferation in endothelial cells. *FASEB J. Off. Publ. Fed. Am. Soc. Exp. Biol.* 23, 3865–3873 (2009).
12. Elmasri H et al. Endothelial cell-fatty acid binding protein 4 promotes angiogenesis: role of stem cell factor/c-kit pathway. Angiogenesis 15, 457–468 (2012). [PubMed: 22562362]
13. Schoors S et al. Fatty acid carbon is essential for dNTP synthesis in endothelial cells. Nature 520, 192–197 (2015). [PubMed: 25830893]
14. Huang H et al. Role of glutamine and interlinked asparagine metabolism in vessel formation. EMBO J. 36, 2334–2352 (2017). [PubMed: 28659375]
15. Kim B, Li J, Jang C & Arany Z Glutamine fuels proliferation but not migration of endothelial cells. EMBO J. 36, 2321–2333 (2017). [PubMed: 28659379]
16. De Smet F, Segura I, De Bock K, Hohensinner PJ & Carmeliet P Mechanisms of vessel branching: filopodia on endothelial tip cells lead the way. *Arterioscler. Thromb. Vasc. Biol.* 29, 639–649 (2009). [PubMed: 19265031]
17. DeBerardinis RJ & Chandel NS Fundamentals of cancer metabolism. *Sci. Adv.* 2, e1600200 (2016). [PubMed: 27386546]
18. Hakkaart GAJ, Dassa EP, Jacobs HT & Rustin P Allotopic expression of a mitochondrial alternative oxidase confers cyanide resistance to human cell respiration. EMBO Rep. 7, 341–345 (2006). [PubMed: 16322757]
19. Perales-Clemente E et al. Restoration of electron transport without proton pumping in mammalian mitochondria. *Proc. Natl. Acad. Sci. U. S. A.* 105, 18735–18739 (2008). [PubMed: 19020091]
20. Sullivan LB et al. Supporting Aspartate Biosynthesis Is an Essential Function of Respiration in Proliferating Cells. Cell 162, 552–563 (2015). [PubMed: 26232225]
21. Titov DV et al. Complementation of mitochondrial electron transport chain by manipulation of the NAD+/NADH ratio. Science 352, 231–235 (2016). [PubMed: 27124460]
22. Birsoy K et al. An Essential Role of the Mitochondrial Electron Transport Chain in Cell Proliferation Is to Enable Aspartate Synthesis. Cell 162, 540–551 (2015). [PubMed: 26232224]
23. King MP & Attardi G Human cells lacking mtDNA: repopulation with exogenous mitochondria by complementation. Science 246, 500–503 (1989). [PubMed: 2814477]
24. Ansó E et al. The mitochondrial respiratory chain is essential for haematopoietic stem cell function. *Nat. Cell* Biol. 19, 614–625 (2017). [PubMed: 28504706]
25. Martínez-Reyes I et al. TCA Cycle and Mitochondrial Membrane Potential Are Necessary for Diverse Biological Functions. Mol. Cell 61, 199–209 (2016). [PubMed: 26725009]
26. Xiao M et al. Inhibition of α-KG-dependent histone and DNA demethylases by fumarate and succinate that are accumulated in mutations of FH and SDH tumor suppressors. Genes Dev. 26, 1326–1338 (2012). [PubMed: 22677546]
27. Xu W et al. Oncometabolite 2-hydroxyglutarate is a competitive inhibitor of α-ketoglutarate-dependent dioxygenases. Cancer Cell 19, 17–30 (2011). [PubMed: 21251613]
28. Wong BW et al. The role of fatty acid β-oxidation in lymphangiogenesis. Nature 542, 49–54 (2017). [PubMed: 28024299]
29. Benedito R et al. The notch ligands Dll4 and Jagged1 have opposing effects on angiogenesis. Cell 137, 1124–1135 (2009). [PubMed: 19524514]

30. Amaya CN & Bryan BA Differential Expression of Angiogenic Gene Networks during Post-natal Lung Alveolarization. Angiol. Open Acce*ss* 4, (2016).
31. Jovaisaite V, Mouchiroud L & Auwerx J The mitochondrial unfolded protein response, a conserved stress response pathway with implications in health and disease. *J. Exp.* Biol. 217, 137–143 (2014). [PubMed: 24353213]
32. Warner JR, Vilardell J & Sohn JH Economics of Ribosome Biosynthesis. *Cold Spring Harb. Symp. Quant. Bio*l. 66, 567–574 (2001). [PubMed: 12762058]
33. Wilhelm K et al. FOXO1 couples metabolic activity and growth state in the vascular endothelium. Nature 529, 216–220 (2016). [PubMed: 26735015]
34. Garcia-Bermudez J et al. Aspartate is a limiting metabolite for cancer cell proliferation under hypoxia and in tumours. *Nat. Cell* Biol. 20, 775–781 (2018). [PubMed: 29941933]
35. Sullivan LB et al. Aspartate is an endogenous metabolic limitation for tumour growth. *Nat. Cell Bio*l. 20, 782–788 (2018). [PubMed: 29941931]
36. Hellström M et al. Dll4 signalling through Notch1 regulates formation of tip cells during angiogenesis. Nature 445, 776–780 (2007). [PubMed: 17259973]
37. Huang H, Bhat A, Woodnutt G & Lappe R Targeting the ANGPT–TIE2 pathway in malignancy. Nat. Rev. Cancer 10, 575–585 (2010). [PubMed: 20651738]
38. Savant S et al. The Orphan Receptor Tie1 Controls Angiogenesis and Vascular Remodeling by Differentially Regulating Tie2 in Tip and Stalk Cells. Cell Rep. 12, 1761–1773 (2015). [PubMed: 26344773]
39. Weinberg F et al. Mitochondrial metabolism and ROS generation are essential for Kras-mediated tumorigenicity. *Proc. Natl. Acad. Sci.* 107, 8788–8793 (2010). [PubMed: 20421486]
40. Tan AS et al. Mitochondrial Genome Acquisition Restores Respiratory Function and Tumorigenic Potential of Cancer Cells without Mitochondrial DNA. Cell Metab. 21, 81–94 (2015). [PubMed: 25565207]
41. Liu X, Romero IL, Litchfield LM, Lengyel E & Locasale JW Metformin Targets Central Carbon Metabolism and Reveals Mitochondrial Requirements in Human Cancers. Cell Metab. 24, 728–739 (2016). [PubMed: 27746051]
42. Naguib A et al. Mitochondrial Complex I Inhibitors Expose a Vulnerability for Selective Killing of Pten-Null Cells. Cell Rep. 23, 58–67 (2018). [PubMed: 29617673]
43. Wheaton WW et al. Metformin inhibits mitochondrial complex I of cancer cells to reduce tumorigenesis. eLife 3, (2014).
44. Birsoy K et al. Metabolic determinants of cancer cell sensitivity to glucose limitation and biguanides. Nature 508, 108–112 (2014). [PubMed: 24670634]
45. Shackelford DB et al. LKB1 Inactivation Dictates Therapeutic Response of Non-Small Cell Lung Cancer to the Metabolism Drug Phenformin. Cancer Cell 23, 143–158 (2013). [PubMed: 23352126]
46. Guo JY et al. Activated Ras requires autophagy to maintain oxidative metabolism and tumorigenesis. Genes Dev. 25, 460–470 (2011). [PubMed: 21317241]
47. Romero R et al. Keap1 loss promotes Kras-driven lung cancer and results in dependence on glutaminolysis. *Nat. Med.* (2017). doi:10.1038/nm.4407
48. Molina JR et al. An inhibitor of oxidative phosphorylation exploits cancer vulnerability. *Nat. Med.* 24, 1036–1046 (2018). [PubMed: 29892070]
49. Weinberg SE & Chandel NS Targeting mitochondria metabolism for cancer therapy. *Nat. Chem. Biol.* 11, 9–15 (2015). [PubMed: 25517383]
50. Zahalka AH et al. Adrenergic nerves activate an angio-metabolic switch in prostate cancer. Science 358, 321–326 (2017). [PubMed: 29051371]
51. Cannino G et al. Glucose Modulates Respiratory Complex I Activity in Response to Acute Mitochondrial Dysfunction. *J. Biol. Chem.* 287, 38729–38740 (2012). [PubMed: 23007390]
52. Pitulescu ME, Schmidt I, Benedito R & Adams RH Inducible gene targeting in the neonatal vasculature and analysis of retinal angiogenesis in mice. *Nat.* Protoc. 5, 1518–1534 (2010). [PubMed: 20725067]

53. Garcia BA et al. Chemical derivatization of histones for facilitated analysis by mass spectrometry. *Nat. Protoc.* 2, 933–938 (2007). [PubMed: 17446892]

54. Zheng Y, Thomas PM & Kelleher NL Measurement of acetylation turnover at distinct lysines in human histones identifies long-lived acetylation sites. Nat. Commun 4, 2203 (2013). [PubMed: 23892279]

55. Zheng Y, Tipton JD, Thomas PM, Kelleher NL & Sweet SMM Site-specific human histone H3 methylation stability: fast K4me3 turnover. Proteomics 14, 2190–2199 (2014). [PubMed: 24826939]

56. MacLean B et al. Skyline: an open source document editor for creating and analyzing targeted proteomics experiments. *Bioinforma. Oxf.* Engl. 26, 966–968 (2010).

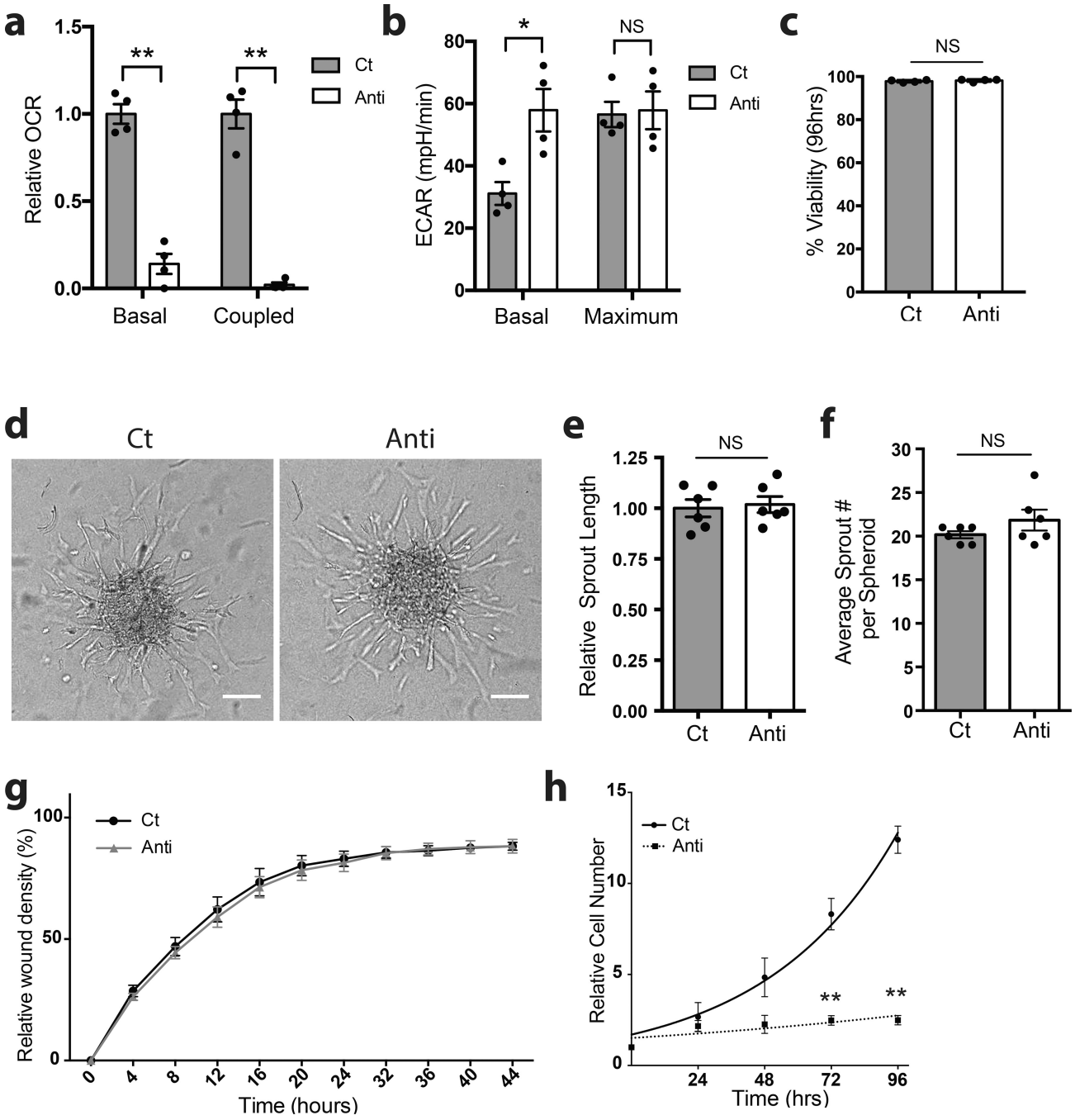

Figure 1: Mitochondrial complex III is required for endothelial cell proliferation *in vitro*

a. Relative basal and coupled oxygen consumption rate (OCR) of control (Ct) or antimycin A (Anti) treated HUVECs, measured after 2 hours treatment. Values are normalized to control mean (n=4 biologically independent experiments). **b.** Basal and maximum extracellular acidification rate (ECAR) of Ct or Anti treated HUVECs, measured after 2 hours treatment (n=4 biologically independent experiments). **c.** Cell viability (% Dapi negative cells) of Ct or Anti treated HUVECs, measured after 96 hours treatment (n=4 biologically independent experiments). **d.** Representative images of Ct or Anti treated

HUVECs in a sprouting assay after 24 hours. Scale bar represents 50μm. Repeated 6 times with similar results. **e.** Quantification of relative sprout length of Ct or Anti treated HUVECs after 24 hours. Values are normalized to control mean (n=6 biologically independent samples). **f.** Quantification of the average number of sprouts per spheroid of Ct or Anti treated HUVECs after 24 hours. (n=6 biologically independent samples). **g.** Relative wound density % over time in a scratch wound migration assay in Ct or Anti treated HUVECs (Ct: n=15; Anti: n=7 biologically independent samples). **h.** Relative cell number in Ct or Anti treated HUVECs at 0, 24, 48, 72, and 96 hours. Cell number relative to number of cells plated on day 0 (n=5 biologically independent experiments). HUVECs were treated with 25nM antimycin A. In sprouting and migration assays, media contained 2ug/mL mitomycin C to inhibit proliferation. Data represents mean +/− SEM and were analyzed with a two-tailed t-test (*$p<0.05$, **$p<0.01$, NS=not significant).

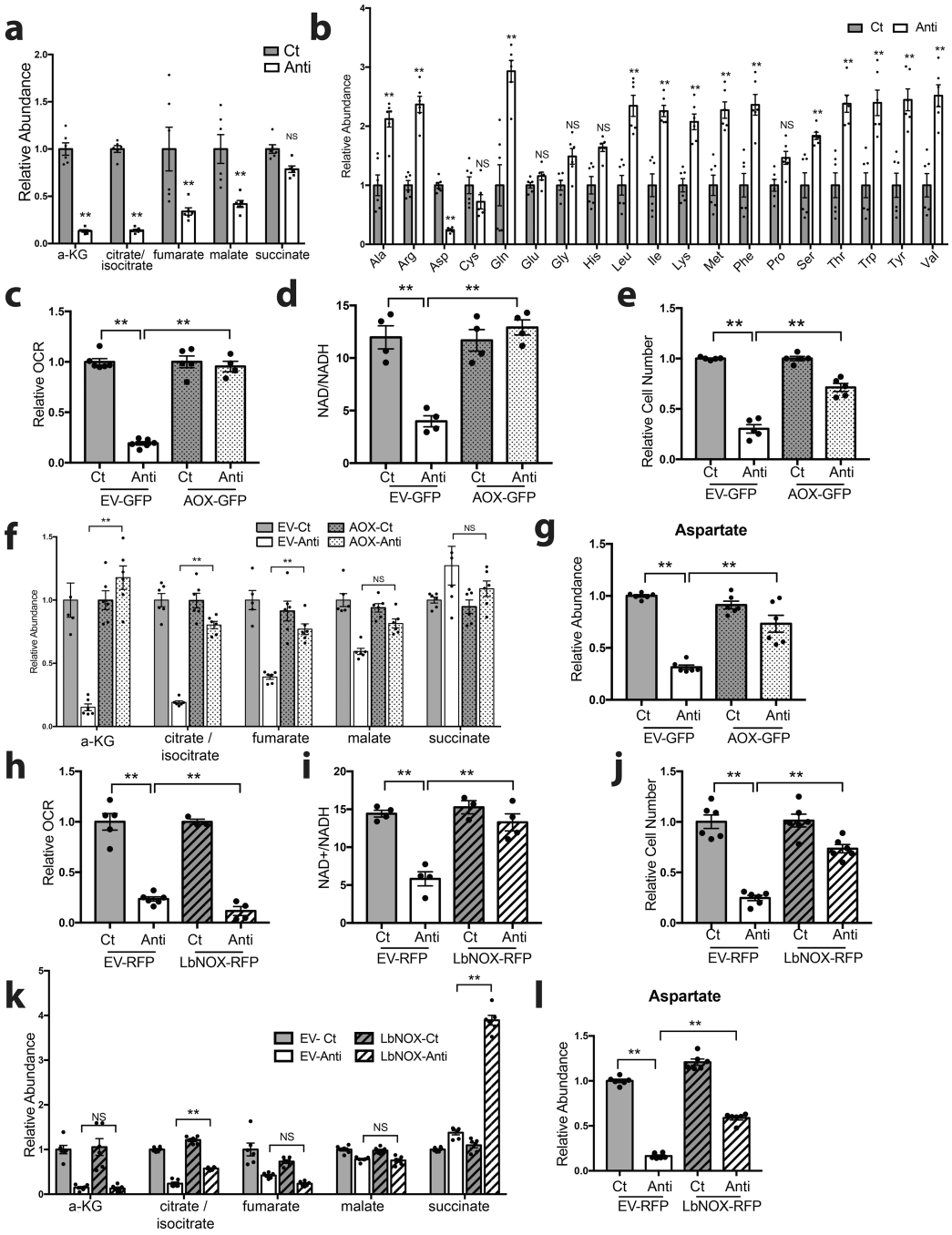

Figure 2: Mitochondrial complex III maintains NAD+/NADH ratio, necessary for endothelial cell proliferation a-b.

Relative abundance of TCA cycle (a), and amino acid (b) metabolites from control (Ct) or antimycin A (Anti) treated HUVECs, after 24 hours treatment. Values are normalized to control mean (n=6 biologically independent experiments). **c.** Relative oxygen consumption (OCR) in empty vector (EV)-GFP or AOX-GFP expressing HUVECs, Ct or Anti treated for 2 hours (representative of n=3 independent experiments). **d.** Ratio of NAD+/NADH in EV-GFP or AOX-GFP expressing HUVECs, Ct or Anti treated for 4 hours (n=4 biologically

independent experiments). **e.** Relative cell number after 72 hours proliferation in EV-GFP or AOX-GFP expressing HUVECs, Ct or Anti treated (n=5 biologically independent experiments). **f-g.** Relative abundance of TCA cycle metabolites (f), and aspartate (g) in EV-GFP or AOX-GFP expressing HUVECs, Ct or Anti treated for 24 hours. Values are normalized to control mean (n=6 biologically independent experiments). **h.** Relative OCR in EV-RFP or LbNOX-RFP expressing HUVECs, Ct or Anti treated for 2 hours (representative of n=3 independent experiments). **i.** Ratio of NAD+/NADH in EV-RFP or LbNOX-RFP expressing HUVECs, Ct or Anti treated for 4 hours (n=4 biologically independent experiments). **j.** Relative cell number after 72 hours proliferation in EV-RFP or LbNOX-RFP expressing HUVECs, Ct or Anti treated (n=6 biologically independent experiments). **k-l.** Relative abundance of TCA cycle metabolites (k), and aspartate (l) in EV-RFP or LbNOX-RFP expressing HUVECs, Ct or Anti treated for 24 hours. Values are normalized to control mean. (n=6 biologically independent experiments). HUVECs were treated with 25nM antimycin A. Data represents mean +/− SEM and were analyzed using one or two-way ANOVA and Tukey's multiple comparisons test (*p<0.05, **p<0.01, NS=not significant).

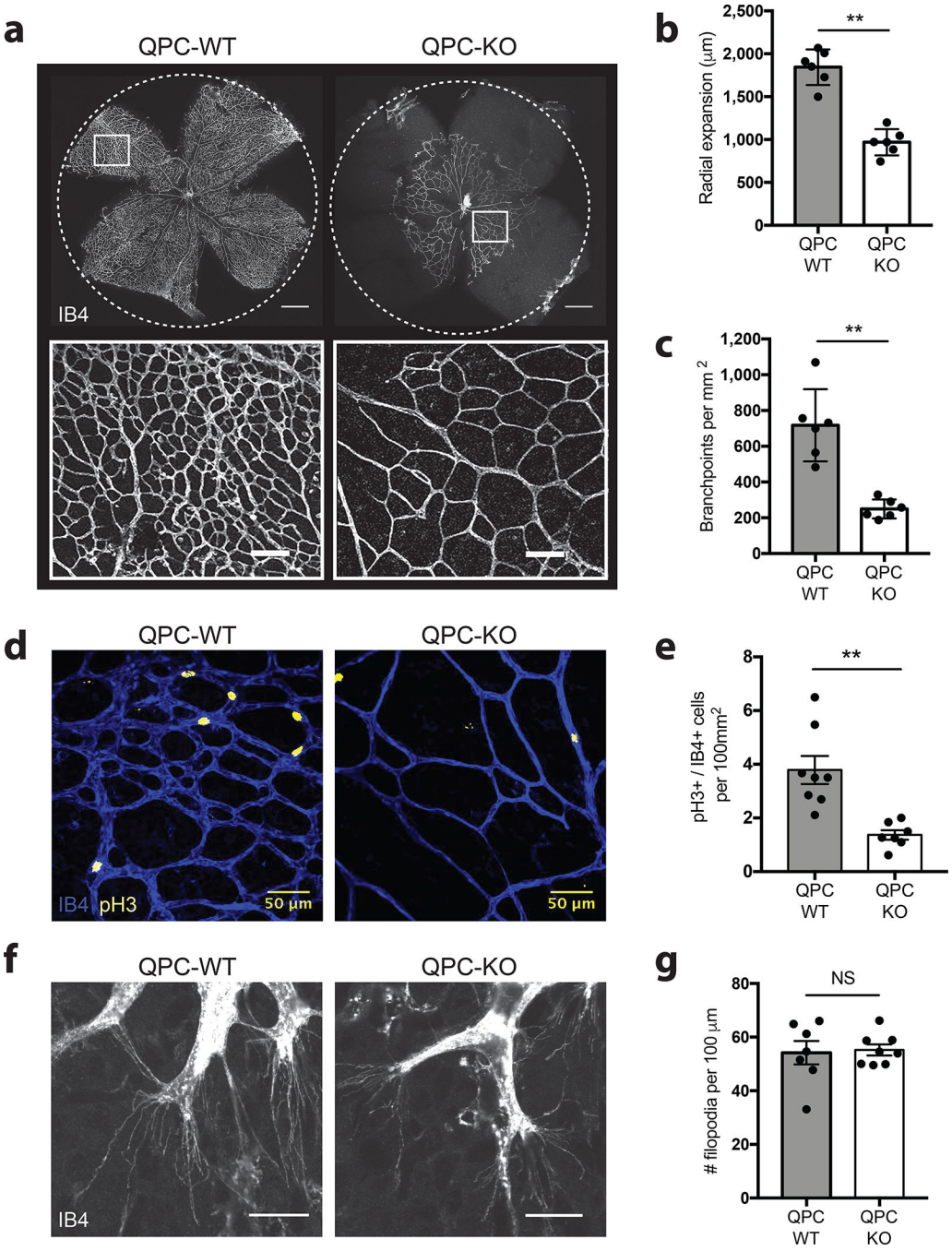

Figure 3: Mitochondrial complex III respiration in ECs is required for post-natal retinal angiogenesis

a. Representative images QPC-WT and –KO retinas stained with isolectin-B4 (IB4) at 10× original magnification. Top panels: Dotted circle represents the QPC-WT radial expansion. Scale bars represents 500μm. Bottom panels: zoomed image representing white box from top panel. Scale bar represents 100μm. **b.** Quantification of radial expansion in QPC-WT and –KO retinas (WT: n=6; KO: n=6 mice). **c.** Quantification of the number of branchpoints per mm^2 in QPC-WT and –KO retinas (WT: n=6; KO: n=6 mice). **d.** Representative images of

QPC-WT and -KO retinas stained with IB4 (blue) and phospo-histone 3 (pH3) (yellow) taken at 40× magnification. Scale bars represent 50μm. **e.** Quantification of pH3+/IB4+ ECs per 100mm^2 (WT: n=8; KO: n=7 mice). **f.** Representative images of filopodia from QPC-WT and –KO retinas stained with IB4 taken at 100× magnification. Scale bars represent 20μm. **g.** Quantification of the number of filopodia per 100μm at the outer retinal edge. (WT: n=7; KO: n=8 mice). Data represent whole-mounted retinas from QPC-WT and –KO post-natal day 7 (P7) pups treated with tamoxifen (P0-P4). Data represents mean +/− SEM and were analyzed with a two-tailed t-test (*p<0.05, **p<0.01, NS=not significant).

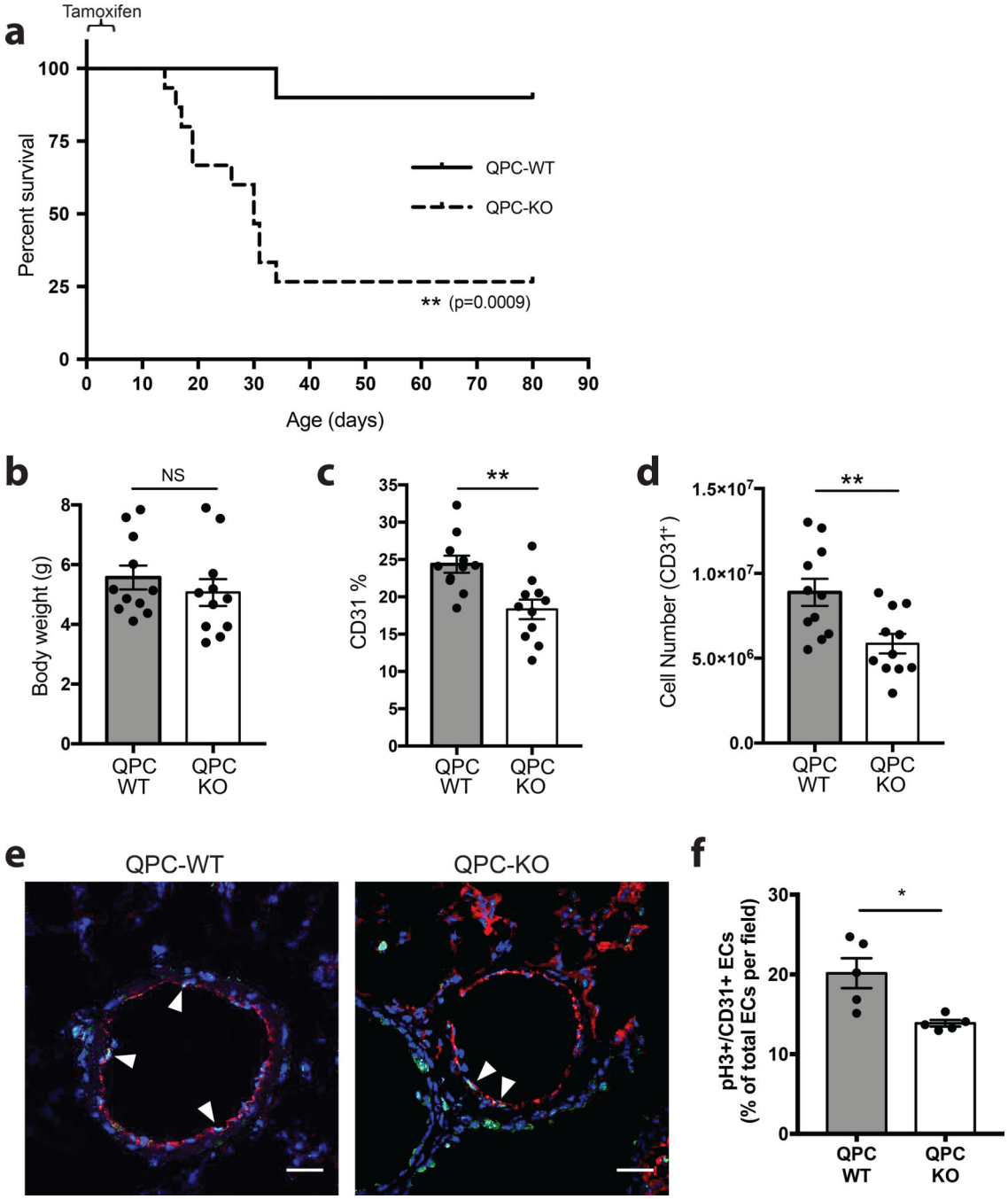

Figure 4: Mitochondrial complex III respiration in ECs is necessary for developmental angiogenesis

a. Survival curve of QPC-WT and -KO pups treated with tamoxifen (P0-P4) (WT: n=10; KO: n=15 mice). **b.** Body weight of QPC-WT and -KO P15 pups (WT: n=11; KO: n=11). **c-d.** Percentage of CD31+ cells (c), and total number of CD31+ cells (d) from the lung of QPC-WT and -KO P15 pups (WT: n=11; KO: n=11 mice). **e.** Representative images of QPC-WT and –KO lung vessels from P15 pups. Vessels stained with CD31 (red), proliferating cells stained with phospho-histone 3 (pH3) (green) and nuclei stained with

DAPI (blue), taken at 60× magnification. Scale bars represent 25μm. White arrows represent pH3+/CD31+ cells. **f.** Quantification of the number of pH3+/CD31+ cells as a percentage of the total number of CD31+ cells counted per vessel in QPC-WT and –KO lung sections (WT: n=5; KO: n=5 mice). Bar graphs represent mean +/− SEM and were analyzed with a two-tailed t-test. Survival curve was analyzed using a Log-rank (Mantel-Cox) test. (*p<0.05, **p<0.01, NS=not significant).

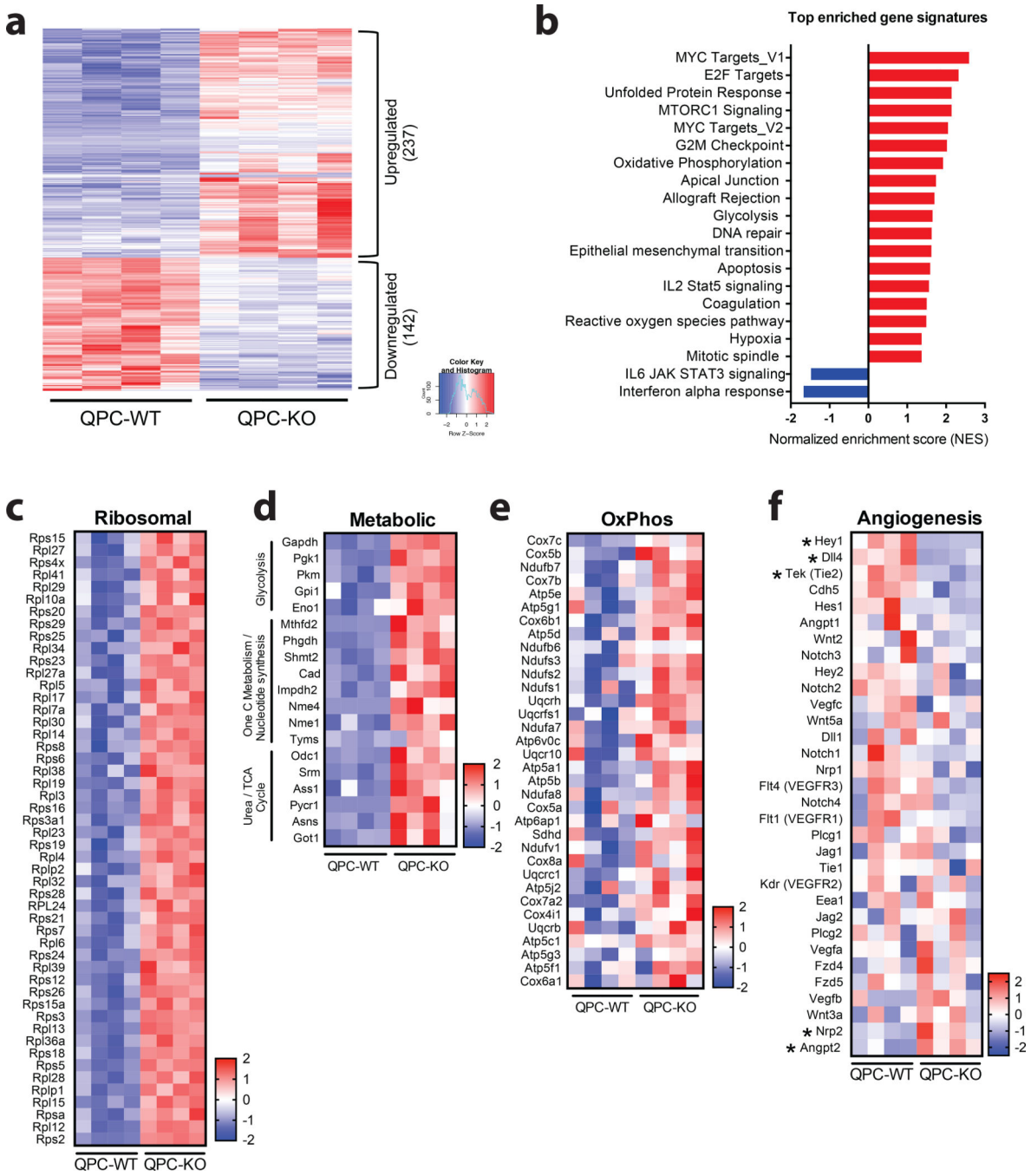

Figure 5: Loss of mitochondrial complex III function in ECs increases anabolic-associated gene expression

a. Heat map of RNA sequencing data representing significantly upregulated (237) and downregulated (142) genes from QPC-WT and -KO P15 lung ECs from pups treated with tamoxifen (P0-P4) (FDR ≤ 0.01). **b.** Gene set enrichment analysis showing top gene signatures upregulated (red) or downregulated (blue) from QPC-WT and -KO P15 lung ECs (NOM p-value ≤ 0.05). **c.** Heat map of RNA sequencing data showing significantly upregulated ribosomal genes from QPC-KO versus -WT P15 lung ECs (FDR ≤ 0.01). **d.**

Heatmap of RNA sequencing data showing significantly upregulated metabolic genes from QPC-WT and –KO P15 lung ECs (FDR ≤ 0.01). **e.** Heat map of RNA sequencing data showing oxidative phosphorylation (OxPhos) genes from QPC-WT and -KO P15 lung ECs. **f.** Heat map of RNA sequencing data showing angiogenic signaling gene expression. * represents genes that are significantly differentially expressed in QPC-KO vs -WT P15 lung ECs (FDR ≤ 0.01). Data shown in heat maps is representative of the z-score. WT: n=4; KO: n=4 mice.

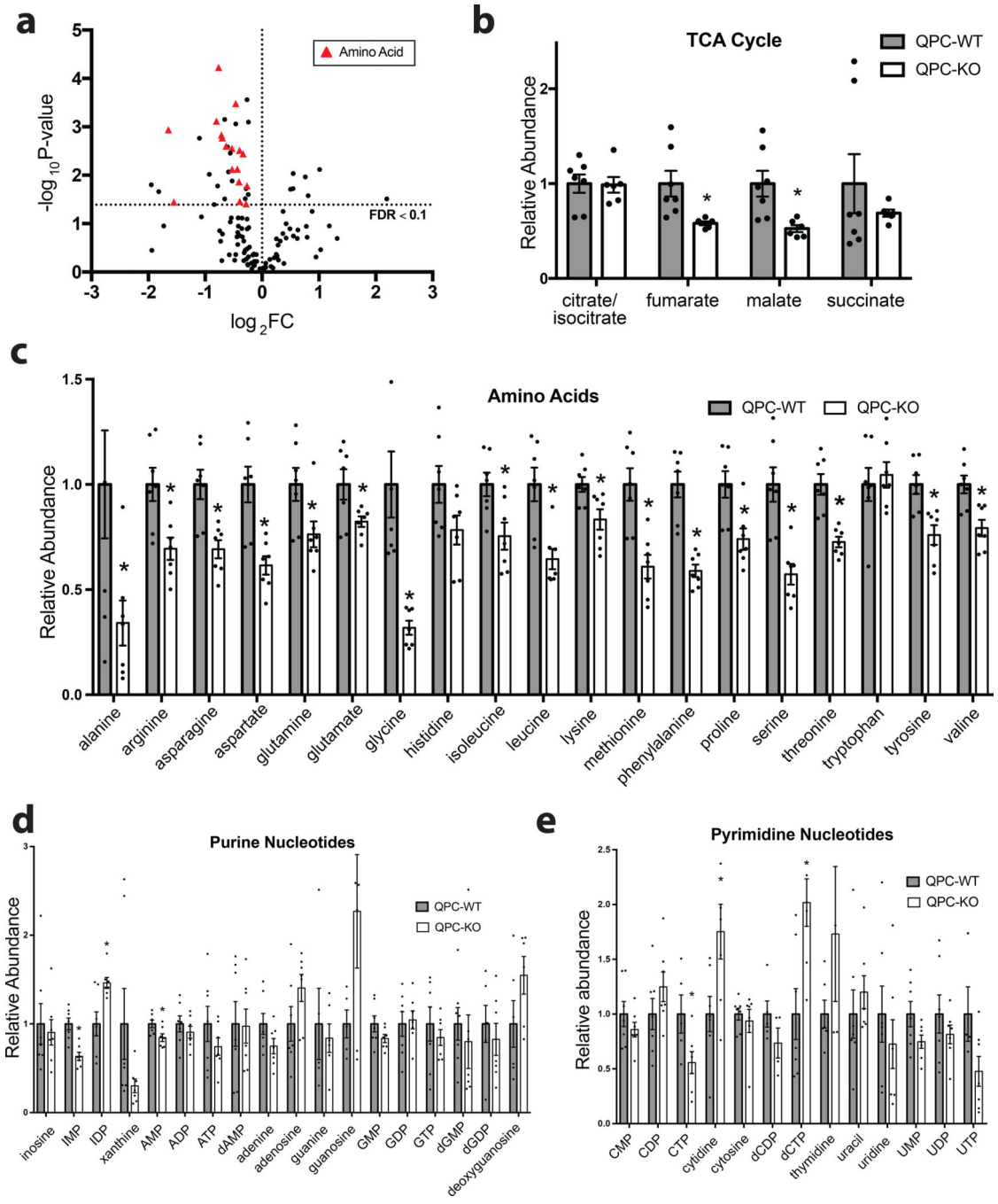

Figure 6: Mitochondrial complex III in ECs is necessary to maintain amino acid levels *in vivo*

a. Volcano plot representing metabolites that are over or under represented in QPC-KO P15 lung ECs versus –WT from pups treated with tamoxifen (P0-P4). Red triangles represent amino acid metabolites (WT: n=7; KO: n=7 mice). **b-e.** Relative abundance of TCA cycle (b), amino acid (c), purine nucleotide (d), and pyrimidine nucleotide (e) metabolites from P15 QPC-WT and –KO lung ECs (WT: n=7; KO: n=7 mice). Data are normalized to QPC-WT mean. Bar graphs represent mean +/− SEM and were analyzed using the Two-stage

linear step-up procedure of Benjamini, Krieger and Yekutieli, with FDR<0.1. (*p<0.05, **p<0.01, NS=not significant).

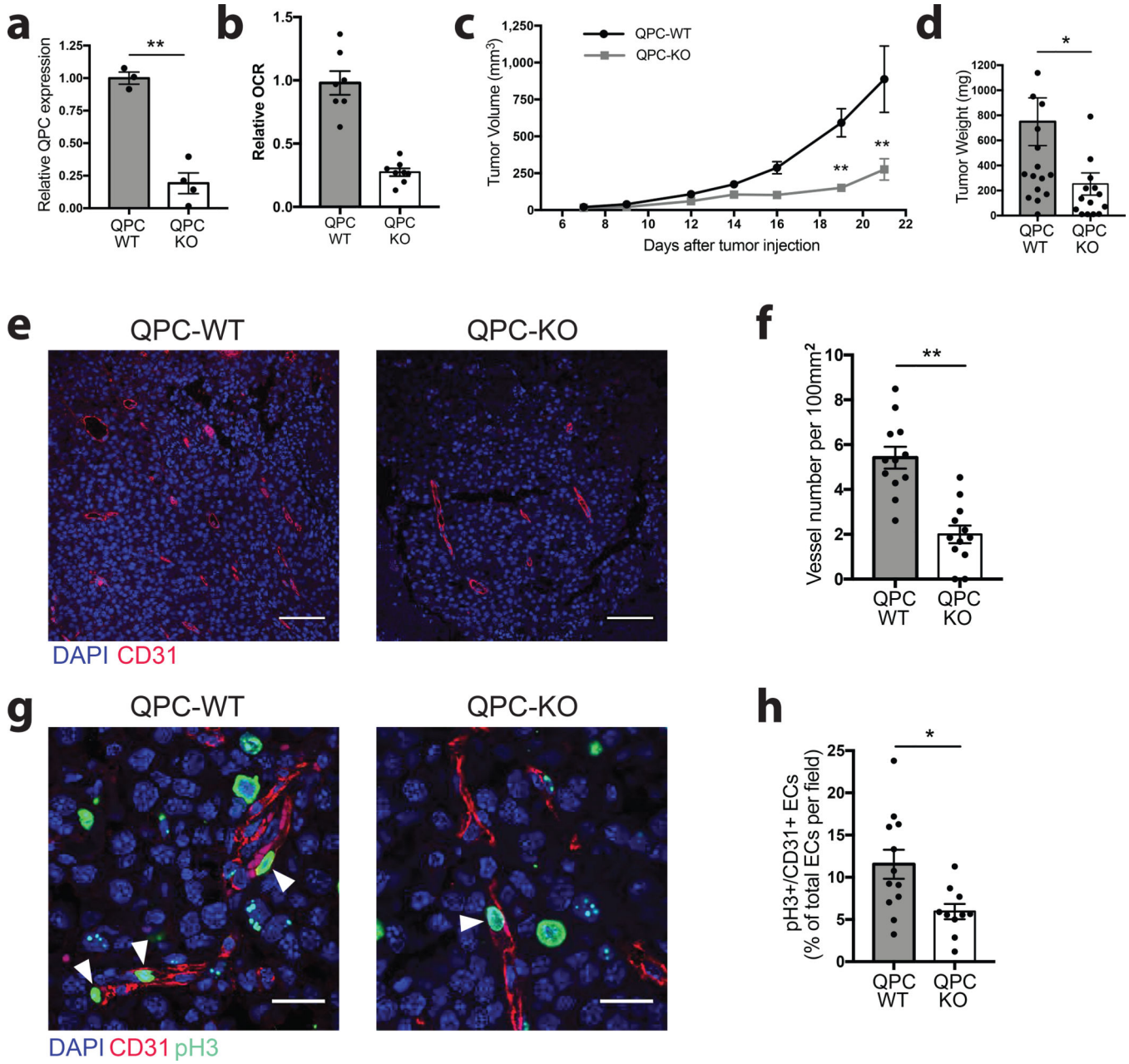

Figrue 7: Mitochondrial complex III respiration in ECs is required for tumor angiogenesis

a. qRT-PCR showing relative QPC expression from QPC-WT and –KO lung ECs from adult mice (WT: n=3; KO: n=4). **b.** Relative basal oxygen consumption (OCR) from QPC-WT and –KO lung ECs (Graph represents WT: n=7 and KO: n=8 technical replicates from WT: n=2; KO: n=2 mice). Error bars represent SEM between technical replicates. **c.** Growth curve of subcutaneous B16-F10 melanoma tumors in QPC-WT and -KO mice (WT: n=20; KO: n=15 mice). **d.** Tumor weight (mg) of subcutaneous B16-F10 melanoma tumors from QPC-WT and -KO mice measured 21 days after injection (WT: n=20; KO: n=15 mice). **e.** Representative images of QPC-WT and -KO B16-F10 melanoma tumor sections. Vessels stained with CD31 (red) and nuclei stained with DAPI (blue), taken at 20× magnification.

Scale bar represents 100μm. **f.** Quantification of the number of vessels per 100mm^2 in QPC-WT and –KO tumor sections (WT: n=12; KO: n=12 mice). **g.** Representative images of QPC-WT and –KO B16-F10 melanoma tumor sections. Vessels stained with CD31 (red), proliferating cells stained with phospho-histone 3 (pH3) (green) and nuclei stained with DAPI (blue), taken at 60× magnification. Scale bars represent 25μm. White arrows represent pH3+/CD31+ cells. **h.** Quantification of the number of pH3+/CD31+ cells as a percentage of the total number of CD31+ cells counted per field in QPC-WT and –KO tumor sections (WT: n=12; KO: n=12 mice). Mice were fed tamoxifen chow for 2 weeks to induce loss of QPC prior to tumor injections and remained on tamoxifen chow for the duration of the experiment. Data represents mean +/− SEM and were analyzed with a two-tailed t-test (*$p<0.05$, **$p<0.01$, NS=not significant).